

Theoretical calculations of CH₄ and H₂ associative desorption from Ni(111): Could subsurface hydrogen play an important role?

Graeme Henkelman^{a)}

Department of Chemistry and Biochemistry, The University of Texas at Austin, Austin, Texas 78712-0165

Andri Arnaldsson

Department of Chemistry, P.O. Box 351700, University of Washington, Seattle, Washington 98195-1700

Hannes Jónsson

Department of Chemistry, P.O. Box 351700, University of Washington, Seattle, Washington 98195-1700 and Faculty of Science, VR-II, University of Iceland, 107 Reykjavík, Iceland

(Received 25 August 2005; accepted 1 December 2005; published online 27 January 2006)

The results of theoretical calculations of associative desorption of CH₄ and H₂ from the Ni(111) surface are presented. Both minimum-energy paths and classical dynamics trajectories were generated using density-functional theory to estimate the energy and atomic forces. In particular, the recombination of a subsurface H atom with adsorbed CH₃ (methyl) or H at the surface was studied. The calculations do not show any evidence for enhanced CH₄ formation as the H atom emerges from the subsurface site. In fact, there is no minimum-energy path for such a concerted process on the energy surface. Dynamical trajectories started at the transition state for the H-atom hop from subsurface to surface site also did not lead to direct formation of a methane molecule but rather led to the formation of a thermally excited H atom and CH₃ group bound to the surface. The formation (as well as rupture) of the H–H and C–H bonds only occurs on the exposed side of a surface Ni atom. The transition states are quite similar for the two molecules, except that in the case of the C–H bond, the underlying Ni atom rises out of the surface plane by 0.25 Å. Classical dynamics trajectories started at the transition state for desorption of CH₄ show that 15% of the barrier energy, 0.8 eV, is taken up by Ni atom vibrations, while about 60% goes into translation and 20% into vibration of a desorbing CH₄ molecule. The most important vibrational modes, accounting for 90% of the vibrational energy, are the four high-frequency CH₄ stretches. By time reversibility of the classical trajectories, this means that translational energy is most effective for dissociative adsorption at low-energy characteristic of thermal excitations but energy in stretching modes is also important. Quantum-mechanical tunneling in CH₄ dissociative adsorption and associative desorption is estimated to be important below 200 K and is, therefore, not expected to play an important role under typical conditions. An unexpected mechanism for the rotation of the adsorbed methyl group was discovered and illustrated a strong three-center C–H–Ni contribution to the methyl-surface bonding. © 2006 American Institute of Physics. [DOI: 10.1063/1.2161193]

I. INTRODUCTION

The critical step in the transformation of methane to more valuable chemicals is the dissociative adsorption on the surface of the catalyst to form an adsorbed methyl group CH₃ and an adsorbed hydrogen atom. Much of the experimental and theoretical work has focused on this step. The most recent and most reliable measurements of the activation energy barrier for dissociative adsorption of CH₄ on Ni(111) give a value of 0.77 ± 0.10 eV.¹ Great care was taken in these measurements to block defects on the surface with unreactive Au atoms and to thermalize the methane gas with the surface. Previous measurements had given a smaller value of 0.55 eV.²

Theoretical studies of the dissociative adsorption have employed various techniques for describing the energetics and have given estimates of the rate within harmonic transi-

tion state theory where the saddle point on the energy surface between the energy minimum corresponding to the methane molecule and the adsorbed methyl group and hydrogen atom gives the activation energy barrier for the transition. Yang and Witten have used cluster models of the surface and calculated the energetics using Hartree-Fock and configuration-interaction (CI) methods.³ Their best estimate of the activation energy for dissociative adsorption is 0.72 eV. The distance between the C atom and the closest Ni atom at the saddle point is 2.41 Å. Bengaard *et al.* have employed density-functional theory methods using both the PW91 and RPBE functionals, obtaining activation energies of 0.73 and 1.05 eV, respectively.⁴ The minimum-energy path for dissociative adsorption is, of course, the same as the minimum-energy path for associative adsorption. The calculated minimum-energy path (MEP) with the RPBE functional gives an activation energy of 0.4 eV for associative desorption of methane when starting with H atom and CH₃-group adsorbed on the surface.

^{a)}Electronic mail: henkelman@mail.utexas.edu

A traditional view of surface chemistry assumes that chemical reactions and dissociative chemisorption take place on the outer surface of the catalyst. However, in a series of experiments by Johnson *et al.*⁵ and Daley *et al.*⁶ the presence of subsurface hydrogen was shown to increase the efficiency of CH₃ and ethylene hydrogenation on a Ni(111) surface. Two theoretical studies of methane associative desorption have addressed this issue.^{7,8} In both studies, density-functional theory (DFT) calculations using the PW91 functional were used to study various pathways for the recombination of the subsurface H atom and surface-adsorbed methyl group. Both groups report an activation energy barrier for the direct recombination process suggested by Ledentu *et al.* but in one case the first-order saddle point is reported to be 1.08 eV higher in energy than the initial state,⁷ while in the other study it is reported to be 1.36 eV higher.⁸ The saddle-point geometry is reported to be quite unusual in that the C–Ni distance was very large—2.5 Å in one⁷ and 2.2 Å in the other.⁸ Typically, the catalysis of a chemical reaction by a transition metal requires the overlap of the half-filled *d*-electron orbitals on a transition-metal atom with the molecular orbitals of the chemical and because of the localized nature of the *d* orbitals a typical transition state involves much shorter distances. In both reports it was pointed out that the activation energy barrier for the process starting from surface H and CH₃ is considerably lower in energy, and the increased reactivity when the Ni catalyst is prepared with subsurface H atoms is not due to a new reaction pathway but rather the additional energy given to the initial state of the desorption process by driving the H atoms into subsurface sites.^{7,8}

The reactivity of subsurface deuterium on Ni(111) has been studied by Wright *et al.*^{9,10} Temperature-programmed desorption experiments of D in both subsurface and surface sites show enhanced D₂ associative desorption on Ni(111) at 180 K, as compared to a thermal base line. The angular distribution of desorbing molecules is consistent with subsurface D atoms surfacing at vacant sites and diffusing on the surface before combining to form D₂. No evidence of a direct recombination process was observed.

Because of the surprising and somewhat inconsistent results reported on the direct recombination pathway involving subsurface hydrogen, we decided to look more carefully into this and apply a rigorous method for finding the minimum-energy paths, the nudged elastic band method,¹¹ as well as direct classical dynamics simulations to investigate the possibility of dynamically correlated reactive events.

II. CALCULATIONS

DFT calculations were done with the VASP code,^{12–14} using the PW91 functional,¹⁵ ultrasoft pseudopotentials,¹⁶ and with a plane-wave basis set with a 350 eV cutoff. The nickel surface was represented as a four- or five-layer slab with either a $p(2 \times 2)$ or a $p(3 \times 3)$ cell. The former has four Ni atoms per layer and the latter has nine. Unless otherwise specified, the calculated results given below are for the largest system, five layers with nine atoms each. The bottom two layers of the slab were constrained to their crystal lattice

positions. The Brillouin zone was sampled with a $4 \times 4 \times 1$ *k*-point mesh for the $p(2 \times 2)$ system and a $2 \times 2 \times 1$ mesh for the $p(3 \times 3)$ system. The sensitivity of the calculated barriers to spin polarization, plane-wave energy cutoff, *k*-point sampling, system size, and surface relaxation was tested and discussed in the Appendix.

Classical trajectories were calculated using a combination of DFT evaluation of atomic forces and a Verlet algorithm for the dynamics. A small time step size of 0.2 fs was used to ensure energy conservation. Energy barriers were calculated using the nudged elastic band (NEB) method¹⁷ with the climbing-image modification to rigorously converge on saddle points.^{18,19} Once a minimum-energy path was found, the dimer method²⁰ was used to reconverge saddle points after slab geometry had been changed or when calculation parameters had been changed. For these calculations, a force-based conjugate-gradient method was used to optimize the geometry.²¹ Saddle points and minima were considered converged when the maximum force in every degree of freedom was less than 0.001 eV/Å.

III. RESULTS

The lattice constant for bulk nickel was calculated and found to be 3.52 Å, matching the experimental value. Using this lattice constant, slab geometries were generated with 12 Å of vacuum between the top of the slab and the bottom of its periodic image.

Adsorption at the four high-symmetry binding sites was studied—the face-centered-cubic (fcc) and hexagonal-close-packed (hcp) threefold hollow sites, the bridge site between two surface atoms, and the on-top site above a single nickel atom. Both the H atom and CH₃ have lowest energy at the fcc threefold site. The calculated binding energy of hydrogen was found to be 2.8 eV, matching the experimental binding energy of 2.77 eV measured by Christmann,²² while the binding energy of CH₃ was found to be 1.8 eV. The binding energy at the hcp site is only a few tens of meV lower for both species. For the CH₃ group there is, furthermore, a minimum in the energy surface corresponding to binding on top of a Ni atom but this is 0.3 eV higher than the fcc site. The on-top site was not a local minimum for the hydrogen atom. Neither hydrogen nor methyl showed a local minimum in the energy surface at the bridge site.

Spin polarization is found to be moderately important for binding, decreasing hydrogen's binding energy by 0.1 eV. The bare Ni(111) surface is stabilized with spin polarization to a larger extent than it is with hydrogen bound to it. The reduction in the binding energy as the spin polarization is included is consistent with the fact that the hydrogen-bound Ni(111) system has one less unpaired electron than the bare surface.

A. Subsurface hydrogen

It requires a large amount of energy, 0.6 eV, to drive a H atom from a surface fcc site to a subsurface site. Figure 1 shows the minimum-energy path for hydrogen resurfacing. The activation energy for resurfacing is small, 0.1 eV. This energy profile is consistent with previous calculations by

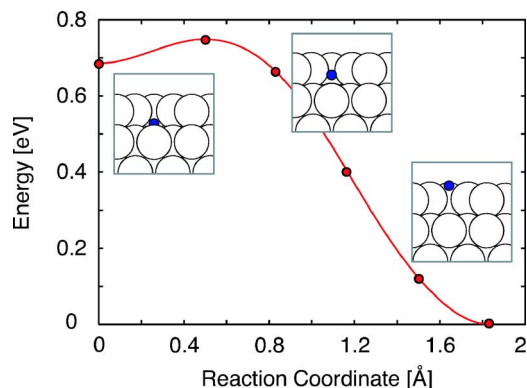


FIG. 1. (Color online) A hydrogen atom is 0.6 eV higher in energy at a subsurface site than at a fcc hollow site at the surface. Hydrogen can resurface with a small energy barrier of 0.1 eV.

Michaelides *et al.*,⁸ Ledentu *et al.*,⁷ and more recently Greeley and Mavrikakis.²³ The energy difference between the surface and subsurface sites makes it very unlikely to find thermal hydrogen in the subsurface layer; at room temperature and low H coverage, for example, it is 10^{10} times less probable. At elevated temperature of 600 K it is over 100 000 times less probable. However, when H₂ gas pressure is high and the H-atom coverage is large, the subsurface sites will be populated to some extent and it is of interest to find out to what extent a reaction mechanism involving subsurface H atoms could contribute to the rate of hydrogenation.

B. H₂ recombination from Ni(111)

To determine the mechanism of subsurface and surface hydrogen recombination, a NEB is constructed with the initial state consisting of atomic surface hydrogen adsorbed in the preferred fcc hollow site^{24,25} directly above a subsurface hydrogen atom (see Fig. 2). The final state consists of the H₂ molecule above the Ni(111) surface beyond the interaction distance. Intermediate images along the NEB [see Fig. 2(a)]

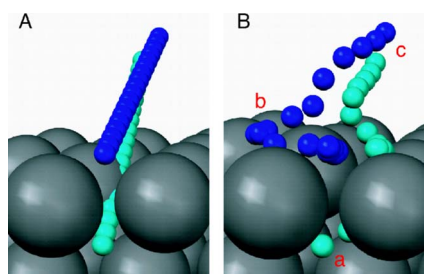


FIG. 2. (Color online) Initial (A) and relaxed (B) nudged elastic band (NEB) for the process by which subsurface hydrogen combines with surface hydrogen to form a gas phase H₂ molecule above the Ni(111) surface. The initial NEB is a linear interpolation between a relaxed geometry in which the surface hydrogen is adsorbed in the fcc hollow site directly above the subsurface hydrogen and a relaxed geometry in which the H₂ molecule is above the surface beyond the interaction distance. The linearly interpolated initial band is an approximation to a direct recombination process but when the NEB relaxes, no such process is found. Instead, the NEB converges to a much more complicated path in which the subsurface hydrogen (a) first diffuses to a neighboring subsurface site so that it can surface at an unoccupied site. The other hydrogen atom (b) then moves to an adjacent surface site so it can recombine with the first over a surface nickel atom to form H₂ (c).

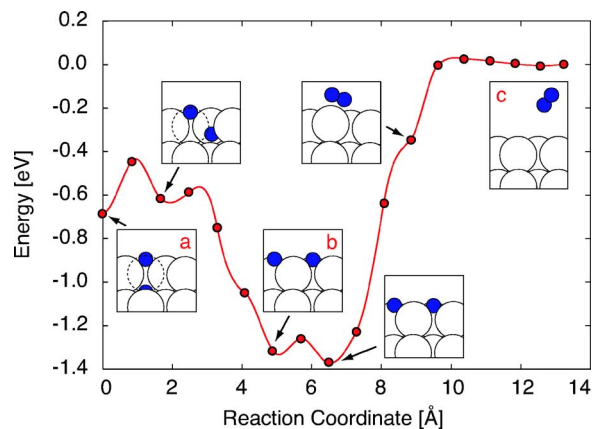


FIG. 3. (Color online) The minimum-energy path for H₂ formation from a subsurface and surface CH₃ group at the Ni(111) surface. The process involves multiple steps. A NEB is constructed with an initial state (a) consisting of a surface hydrogen atom in the lowest-energy hollow site on Ni(111) directly above a subsurface hydrogen and a final state (c) consisting of the H₂ molecule above the metal surface. The NEB does not find a direct recombination mechanism. Instead, the minimum-energy path breaks up into a set of processes. First the subsurface hydrogen moves to an adjacent subsurface site, allowing it to surface in an unoccupied site (b). Two hydrogen atoms then move to neighboring surface sites, one in the fcc and the other in the hcp hollow, so that the H₂ molecule (c) can recombine on the exposed side of a Ni surface atom.

are placed linearly between the initial and final states. The linear interpolation is a good estimate of the direct recombination process. The fact that the NEB converges to a completely different path (see Figs. 2 and 3) shows that there is no direct recombination process. Rather, the hydrogen molecule wants to recombine on the exposed side of a nickel atom. In order for the NEB to cross this transition state and satisfy the initial- and final-state constraints, several intermediate minima appear (automatically) along the band. First, the subsurface hydrogen moves to an adjacent subsurface site (position a in Figs. 2 and 3), so that it can emerge at an unoccupied surface site. At this point the two hydrogen atoms are directly across a surface nickel atom (position b in Figs. 2 and 3), requiring one hydrogen atom to move to an adjacent surface site so that the H₂ molecule can recombine (position c in Figs. 2 and 3) on the exposed side of the surface nickel atom.

Considering the reverse process, a dissociative adsorption reaction can simplify the description. The H₂ molecule dissociates over a surface nickel atom into adjacent surface sites. The rest of the process is simply required to move the hydrogen atoms to the specific final state in which a subsurface hydrogen atom is directly below a hydrogen atom adsorbed in a fcc hollow site.

C. CH₄ recombination from Ni(111)

The role of subsurface hydrogen in the recombination process with methyl on Ni(111) was investigated in the same manner as H₂. Figure 4 shows a converged NEB with an initial state consisting of the methyl group in a hollow site directly above hydrogen in a subsurface site and a final state with methane above the surface. Just as with H₂ recombination, no direct recombination process with subsurface hydrogen is found. Instead the NEB breaks up into a set of inter-

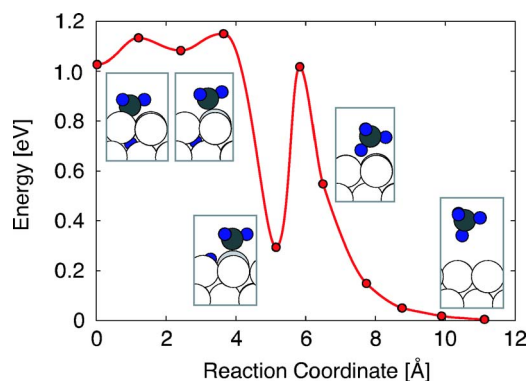


FIG. 4. (Color online) The minimum-energy path for CH_4 formation from a subsurface H atom and surface H atoms at the Ni(111) surface. The process involves multiple steps. The first step involves the methyl group hopping to an on-top site. Then the subsurface hydrogen hops to the surface. In the second step, methyl recombines with the surface hydrogen on the exposed surface of the raised Ni atom.

mediate processes. First the methyl molecule moves to an on-top site which allows the subsurface hydrogen atom to surface into an unoccupied hollow site. Then, as with H_2 , recombination takes place on the exposed side of a surface nickel atom. Figure 5 shows this three-step recombination process.

These calculations show that there is no direct mechanism for methyl recombination with subsurface hydrogen. The experimental evidence for the importance of subsurface hydrogen in methane recombination⁵ is based on a nonequilibrium experiment in which subsurface hydrogen is induced under high pressure, and surface hydrogen is removed with an atomic Xe beam. The observed increase in reactivity does not result from a new and faster mechanism which opens up with the presence of subsurface H atoms but it could be caused by the release of (nonthermal) energy stored in the subsurface hydrogen. We have done *ab initio* molecular-

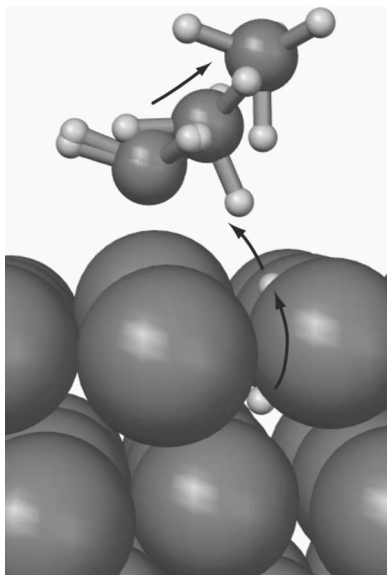


FIG. 5. Graphical representation of the methyl recombination process showing hydrogen resurfacing before recombining with methyl over a nickel surface atom.

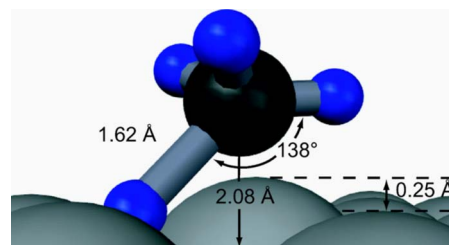


FIG. 6. (Color online) Geometry of the saddle point for methyl recombination (and dissociation) on the surface of Ni(111). The methyl group and the surface hydrogen react on the exposed side of a single-raised surface Ni atom. The Ni atom is raised by 0.25 Å at the transition state. It is likely that the upward displacement of this atom raises the energy of the Ni *d* bands to favor bonding with the methyl group and reduce the barrier energy (Ref. 26).

dynamics simulations to test this. This is described in Sec. III E.

The only theoretically observed mechanism for the dissociative adsorption of methane on Ni(111) involves methyl and hydrogen adsorbing onto the surface. Our most accurate simulation with a five-layer, nine-atom-per-layer Ni(111) slab with three relaxed layers, a 350 eV plane-wave energy cutoff, a $2 \times 2 \times 1$ Monkhost-Pack *k*-point mesh, including spin polarization has a barrier of 0.82 eV. This is in excellent agreement with the barrier of 0.77 eV obtained in recent experiments by Egeberg *et al.*¹

The transition state geometry, shown in Fig. 6, shows a remarkable nickel atom surface relaxation of 0.25 Å. The atom rises out of the surface to provide a favorable environment for the hydrogen-methyl bond-breaking reaction. This was first observed in calculations of methane dissociation on Ir(111),²⁷ and then for methane on Ni(111) by Bengaard *et al.*⁴ The surface relaxation is moderately important for the reaction barrier; methane reacting on a frozen surface has a barrier which is 0.14 eV higher. Mavrikakis *et al.*²⁶ have suggested that a strained surface can raise the energy of the *d*-band electron energy levels to enhance reactivity. The effect of surface relaxation on the barrier energy is less dramatic than that reported in Ref. 27 because the saddle-point calculations on Ir(111) were not converged with respect to *k*-point sampling.²⁸

D. Partitioning of CH_4 desorption energy

One of the intriguing possibilities suggested originally from the work of Polanyi and Wong²⁹ is state-specific chemistry. If it is known which modes need to be excited in order to make molecules overcome a reaction barrier, there is the possibility of injecting energy into just those modes to enhance reactivity. In order to address this question for the methane dissociative adsorption reaction, a dynamics simulation was run starting from the saddle point for desorption. The molecule was moved a small (0.1 Å) distance away from the surface so that it desorbed from the surface during the simulation. A calculation of 150 fs was sufficient to reach a CH_4 -surface distance of 5.3 Å, where the molecule is no longer interacting with the surface at this level of theory. It was then possible, by looking at the velocity of each atom in the system, to partition the energy into different modes of the

TABLE I. Energy distribution of the CH₄ molecule as it leaves the Ni(111) surface. A 1 ps *ab initio* molecular-dynamics simulation is started from the saddle point for methane dissociation, slightly displaced away from the surface so that the methane molecule desorbs from the surface. The 0.82 eV potential energy at the saddle (0.85 after being displaced) is partitioned into translation, rotation, internal energy of the CH₄ molecule, and energy that is left behind in the nickel surface.

Energy (eV)	Mode or subsystem
0.13	Ni(111) slab
0.50	CH ₄ translation
0.03	CH ₄ rotation
0.19	CH ₄ vibration
0.85	Total in CH ₄ and Ni(111) systems

system as the molecule leaves the surface. Such a partitioning is shown in Table I. The majority (59%) of the saddle-point energy goes into translational energy of the methane molecule, making that the most important degree of freedom for dissociative adsorption. Further 22% and 4% of the energy go into vibrational and rotational energies of CH₄, respectively. The final 15% of the energy is left behind in vibrational motion of the nickel atoms.

It was also possible to subdivide the internal CH₄ energy into its internal modes. To do this, the dynamical simulations were continued for 200 fs after the methane molecule was no longer interacting with the surface. The velocity of the molecule at each time step was projected onto the normal modes of the molecule. The kinetic energy in each mode could then be calculated, and the total energy can be found by the virial theorem. The average energy in each mode is reported in Table II along with the calculated frequency, symmetry, degeneracy, and description of each mode. The CH₄ normal modes were calculated at the MP2 level using the GAUSSIAN98 software.³⁰ The frequencies, obtained with MP2 and a local basis set, were significantly closer to the experimental values than could be calculated with the periodic VASP code using a plane-wave basis set.

Table II shows that the high-frequency stretch modes contain 88% of the vibrational energy of the desorbing CH₄ molecule. This energy is only ca. 1/20 of the vibrational quantum so these classical dynamics cannot be expected to give an accurate description of the vibrational motion of the CH₄ molecule. Our results do, however, suggest that the stretching modes are more important than the lower-frequency deformation modes, and that there could be some enhancement of the dissociation rate if adsorbing methane molecules could be prepared with high energy in the stretch-

TABLE II. Vibrational energy of a desorbing CH₄ molecule projected onto the normal modes. An averaging over 200 fs was calculated. This analysis suggests that energy in the symmetric and asymmetric stretch modes can equally enhance dissociative adsorption.

Energy (eV)	Mode Description	Frequency (cm ⁻¹)
0.021	T ₂ (×3) asymmetric stretch	3207
0.020	A ₁ (×1) symmetric stretch	3063
0.003	E(×2) asymmetric deformation	1551
0.002	T ₂ (×3) asymmetric deformation	1324

ing modes and a high translational kinetic energy. Evidence of this enhancement was recently observed by Smith *et al.*³¹ and Juurlink *et al.*³²

E. Classical dynamics trajectories of H resurfacing near adsorbed CH₃

It is evident from the NEB calculations that there does not exist a direct recombination mechanism for a subsurface hydrogen atom and an adsorbed methyl group on the Ni(111) surface. It is, however, possible that the energy released (0.6 eV) when a hydrogen atom resurfaces enhances the CH₄ dissociation rate. Since the energy barrier for resurfacing is low (ca. 0.15 eV) we were able to run a classical dynamics simulation at 500 K to see what happens when the hydrogen resurfaces.

An initial geometry was chosen with a subsurface hydrogen atom directly below an adsorbed methyl in the hollow site of Ni(111). One methyl molecule on our nine-atom-per-layer Ni surface corresponds to a 1/3 coverage, assuming that methyl molecules can occupy 1/3 of the fcc sites in a full monolayer. This configuration was chosen to maximize the chance of seeing a direct recombination event. A velocity scaling thermostat was used to generate a set of independent coordinates and velocities consistent with a temperature of 500 K. Fourteen such geometries were used as initial configurations to generate dynamics trajectories of 8.5 ps (or until a reactive event took place), using a time step of 0.2 fs. Temperature was controlled with a weak Nosé thermostat, using a coupling mass of 5 amu.

During the dynamics runs, the methyl and subsurface hydrogen atom oscillated in their original potential basins until either the methyl group or hydrogen atom hopped to a neighboring site. This typically happened several times before a surfacing event occurs, and the species may have accumulated a considerable distance from each other when finally such an event takes place. A surfacing event where the methyl group was in the hollow site or in an on-top site adjacent to the hollow site where the hydrogen atom emerged was never observed. On average, a surfacing event took place every 4.5 ps. This time scale is consistent with a harmonic transition state theory estimate of the rate, a reaction barrier of 0.15 eV will be crossed on average after 6.5 ps at a temperature of 500 K, assuming a typical reaction prefactor of $5 \times 10^{12} \text{ s}^{-1}$. A surfacing event took place in 11 of the 14 trajectories within our time limit of 8.5 ps. Several different mechanisms were seen in these 11 trajectories where surfacing of the hydrogen atom occurred, as described below.

In one trajectory, the CH₃ group dissociated into CH₂ and an adsorbed hydrogen atom, before the subsurface hydrogen hopped to the surface. In three others, the methyl hopped to a neighboring hollow site before the hydrogen surfaced and thermalized. In four, the subsurface hydrogen hopped to an adjacent subsurface site before resurfacing. In the remaining three trajectories both the methyl and the subsurface hydrogen hopped laterally before the resurfacing event took place. In each case, the resurfacing hydrogen did not show any sign of recombining with the methyl group.

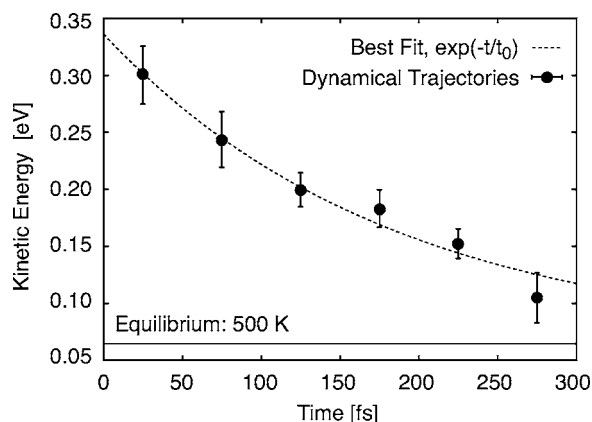


FIG. 7. Block-averaged kinetic energy for the surfacing H atom. The first 300 fs after the H atom crosses the surface plane are broken into six 50 fs segments and averaged over each one. The error bars are the normalized standard deviation for each segment. An exponential fit to these data shows a relaxation time t_0 of 200 fs. This is expected to be an underestimation of the true relaxation time because we have used classical dynamics with a weak thermostat. These calculations show that a resurfacing H atom will be hot due to the release of 0.6 eV of potential energy, but that this energy is dissipated to the substrate on the picosecond time scale.

Instead, the resurfacing energy was transferred into the kinetic energy of the hydrogen atom, which was dissipated to the surface on a time scale of 200 fs (shown in Fig. 7).

This relaxation time is somewhat shorter than other calculated and measured lifetimes of hot-adsorbed H atoms on metal surfaces, in part due to a weak thermostat present during the dynamics. Klamroth and Saalfrank calculate a time scale of several picoseconds for adsorbed H atoms to settle into binding sites on Cu(100).³³ In these simulations, it was found that classical dynamics provides an accurate estimate of the energy decay time, as compared to full wave-packet dynamics. Strömquist *et al.*³⁴ have done classical dynamics simulations of H/Cu(111) using a model energy landscape fit to *ab initio* data and found an energy relaxation time of 1.4 ps. Recently, Trail *et al.*³⁵ have found a shorter relaxation time of 0.8 ps from dynamics simulations using forces from DFT. They also estimate that electronic friction, due to electron-hole pair creation, will reduce the relaxation time scale for a H atom on a metal surface by roughly 80% as compared to a Born-Oppenheimer classical dynamics simulation. Infrared reflection adsorption experiments³⁶ have also determined a subpicosecond lifetime of 0.7 ps for H on Cu(111). The agreement between this wide range of computational techniques with experiment provides convincing evidence that energy dissipates from H adatoms to the metal surface on the picosecond time scale.

The lateral diffusion of subsurface hydrogen and the adsorbed methyl molecule away from each other, as observed in the trajectory data, is supported by comparing the energetics between the initial configurations, in which the subsurface hydrogen is directly below the adsorbed methyl group. The energy of this configuration is 0.08 eV higher than the same species at infinite separation. This repulsive interaction between the subsurface H atom and the surface methyl group will reduce the chance of finding a hot hydrogen atom in the vicinity of an adsorbed methyl molecule.

These dynamical trajectories support the suggestion that

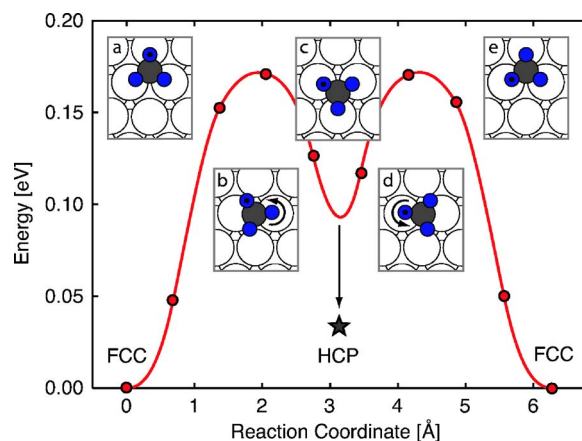


FIG. 8. (Color online) The optimal mechanism for the rotation of a methyl group adsorbed on a Ni(111) surface involves first a displacement of the C atom from a fcc to an adjacent hcp hollow site. During this process, one of the hydrogen atoms maintains contact with an underlying Ni atom. In this intermediate state (indicated by \star), the methyl group has rotated by 60° . In the second step, the methyl group rotates about a different hydrogen atom and the C atom gets displaced back to the original fcc site—completing the 120° rotation. This mechanism, and the high rotational barrier, indicates a strong three-center C–H–Ni interaction.

resurfacing hydrogen is unlikely to increase the CH_4 desorption rate, except by local heating in the case of an athermal subsurface population. In thermal equilibrium, the presence of subsurface hydrogen will not enhance the desorption rate of CH_4 . Furthermore, unless there is a very high density of methyl groups on the surface, it is unlikely that a resurfacing hydrogen atom will find a methyl group in the ca. 200 fs that it takes for the resurfacing energy to dissipate. Both the transition state and dynamics calculations indicate that subsurface hydrogen will not contribute to CH_4 recombination from Ni(111) under thermal catalytic conditions.

F. Methyl diffusion

The interaction of the CH_3 with the surface is of a strong three-center character. The H atoms are strongly attracted to the nearby Ni atoms and the lowest-energy configuration has the three hydrogen atoms pointed towards the adjacent surface nickel atoms. This effect has been discussed by Michaelides and Hu.³⁷ The strength of these bonds was investigated by finding the barrier for rotation of the CH_3 group. A NEB calculation was set up with the CH_3 sitting at a fcc hollow site in both the initial and final states, with the labeling of the H atoms changed to reflect a 120° rotation about the surface normal going through the carbon atom. The initial chain of images was generated by a linear interpolation between the initial and final states. Figure 8 shows the converged minimum-energy path. Remarkably, the hydrogen-metal binding is so strong that CH_3 does not rotate about the carbon atom. Instead, the carbon atom first gets displaced to a hcp site and the CH_3 group rotates 60° about one of the H atoms [see Fig. 8, inset (a)]. In the second step, the carbon atom is displaced back to the fcc site and the CH_3 group rotates by another 60° about another one of the H atoms, as shown in Fig. 8, inset (b). The overall methyl rotation barrier on Ni(111) is 0.17 eV. This illustrates how the

NEB method can find a minimum-energy path that is quite far removed from the initial guess and thereby reveal an unexpected transition mechanism.

G. Quantum effects

Quantum zero-point and tunneling effects have been evaluated for dissociative adsorption of CH₄ on Ni(111) within the harmonic approximation. We have considered the dissociative adsorption process instead of associative desorption because previous studies have most often focused on adsorption.

In classical transition state theory, after making a harmonic approximation for vibrational modes, the rate constant for dissociative adsorption can be written as^{38,39}

$$k_{\text{cl}}^{\text{hTST}} = \frac{1}{Q_{t,r}^{\text{init}}} \frac{\prod_i \nu_i^{\text{init}}}{\prod_i \nu_i^{\ddagger}} e^{-(E^{\ddagger} - E^{\text{init}})/k_B T}, \quad (1)$$

where ν_i^{init} and ν_i^{\ddagger} are the frequencies of harmonic vibrational modes at the initial-state minimum and saddle point, respectively, and $Q_{t,r}^{\text{init}}$ is the product of translational and rotational partition functions of the initial gas phase molecule.

The normal modes of the CH₄ molecule in the gas phase and at the saddle point for dissociative adsorption were evaluated from the DFT forces using a finite difference scheme. The total zero-point energy in the nine vibrational modes of a gas phase CH₄ molecule was found to be 1.23 eV. At the saddle point, the frequencies obtained from small displacements of the C and H atoms while keeping the Ni atoms frozen gave a total zero-point energy of 1.07 eV from the 14 stable vibrational modes. The difference in the zero-point energy of the initial and transition states is commonly used as a correction to the classical activation energy barrier. In this case, such a correction would lower the barrier by 0.16 eV (see Fig. 9). However, this approximation is only valid at low temperature when each vibrational mode is in its ground state.

A better approximation to the quantum-mechanical rate constant can be obtained by using quantum-mechanical partition functions for the vibrational modes in both the initial and transition states while keeping the classical mechanical definition of the normal modes. When the harmonic quantum partition function is used instead of the classical limit, the Wigner correction⁴⁰ to the classical rate constant is obtained,

$$k_{\text{qm}}^{\text{hTST}} = \frac{\prod_i \sinh(x_i^{\text{init}})/x_i^{\text{init}}}{\prod_i \sinh(x_i^{\ddagger})/x_i^{\ddagger}} k_{\text{cl}}^{\text{hTST}}, \quad (2)$$

where $x_i = \hbar \nu_i / 2k_B T$ is the ratio of the zero-point energy to the thermal energy in each vibrational mode. The quantum correction to the classical rate can also be expressed as a temperature-dependent correction to the classical activation energy barrier,

$$k_{\text{qm}}^{\text{hTST}} = e^{-\delta E/k_B T} k_{\text{cl}}^{\text{hTST}}. \quad (3)$$

In the case of the Wigner approximation, the correction to the classical barrier is

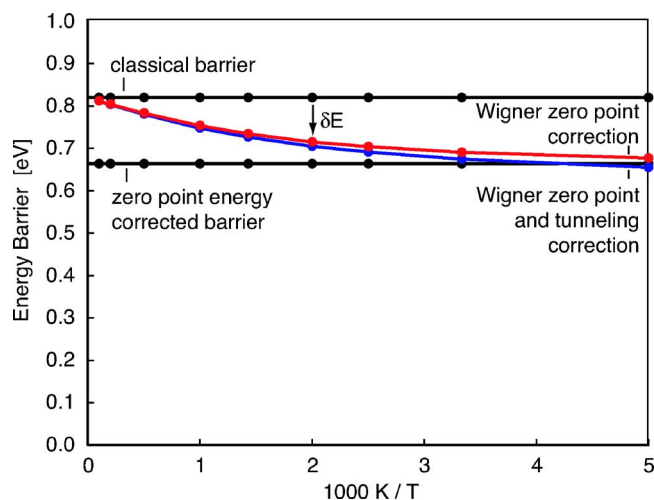


FIG. 9. (Color online) Quantum-mechanical correction δE to the energy barrier for dissociative adsorption of CH₄. The simple, commonly used zero-point energy correction [Eq. (5)] shifts the classical barrier from 0.82 eV (upper line) down to 0.66 eV (lower line). This is a poor approximation at high temperature where the system is not confined to the ground state. The Wigner zero-point energy correction [Eq. (4), shown in red], which treats classical harmonic modes as quantum oscillators, smoothly switches between the simple zero-point corrections at low temperature to the classical barrier at high temperature. The addition of the Wigner tunneling correction [Eq. (6), shown in blue] does not significantly change the barrier above the crossover temperature of 200 K [see Eq. (7)] for this reaction.

$$\delta E_{\text{Wig}} = -k_B T \ln \left[\frac{\prod_i \sinh(x_i^{\text{init}})/x_i^{\text{init}}}{\prod_i \sinh(x_i^{\ddagger})/x_i^{\ddagger}} \right]. \quad (4)$$

In the high-temperature limit, the Wigner correction vanishes, and in the low-temperature limit, it goes to the commonly used zero-point energy correction,

$$\delta E_{\text{zp}} = \sum_i \frac{\hbar \nu_i^{\ddagger}}{2} - \sum_i \frac{\hbar \nu_i^{\text{init}}}{2}. \quad (5)$$

Figure 9 shows a comparison of the classical barrier ($\Delta E = E^{\ddagger} - E^{\text{init}}$), the zero-point-corrected barrier ($\Delta E + \delta E_{\text{zp}}$), and the Wigner-corrected barrier ($\Delta E + \delta E_{\text{Wig}}$) for the CH₄ dissociative adsorption barrier at temperature above 200 K. Plotting the quantum-corrected rate in this way shows at which temperature quantum effects become important, and when the simple zero-point energy correction can be used. At the operating temperature of a typical industrial catalyst, only a fraction of the simple zero-point energy correction is appropriate.

The effect of quantum-mechanical tunneling can also be estimated using a harmonic Wigner correction.⁴¹ The ratio of the rate constant including both tunneling and zero-point energy and the rate constant that only includes zero-point energy quantum effects is

$$k_{\text{qmzpt}}^{\text{hTST}}/k_{\text{qmzp}}^{\text{hTST}} = \frac{\hbar \nu^* / 2k_B T}{\sin(\hbar \nu^* / 2k_B T)} = \frac{x^*}{\sinh x^*}, \quad (6)$$

where ν^* is the imaginary frequency at the saddle point, and $x^* = \hbar \nu^* / 2k_B T$. The correction can only be used above the crossover temperature for tunneling

$$T_c = \frac{\hbar |\nu^*|}{k_B}, \quad (7)$$

at which point the approximation diverges. The crossover temperature for the Wigner approximation is the same as that obtained from the WKB approximation.⁴² Above this crossover temperature, the reaction mechanism can be thought of as over-the-barrier hop, but at lower temperature tunneling is the dominant mechanism. An appealing aspect of the Wigner tunneling correction [Eq. (6)] is that the imaginary frequency at the saddle point ν^* enters into the quantum rate expression [Eq. (2)] in the same way that the real frequencies do in the Wigner zero-point correction. The Wigner correction to the classical barrier [Eq. (4)] includes the tunneling correction [Eq. (6)] if the product over saddle-point modes in the denominator includes the imaginary frequency mode along the reaction coordinate. For CH₄, we find that the imaginary frequency has a magnitude of 850 cm⁻¹ at the saddle point which corresponds to a crossover temperature T_c of 200 K. The small difference between the Wigner corrections with and without tunneling (Fig. 9) shows how small the tunneling correction is above the crossover temperature.

IV. CONCLUSIONS

We have carried out various calculations of associative desorption of H₂ and CH₄ to study, in particular, the role that subsurface H atoms could play in these processes. We have carried out calculations of minimum-energy paths, which are the paths with highest statistical weight in thermal systems, as well as calculations of classical dynamics and energy partitioning between vibrational modes. Although it might seem, judging from steric arguments, that a subsurface H atom could readily react with a surface-adsorbed methyl group or H adatom, a minimum-energy path for such a process was not found. Also, direct classical dynamics simulations of the surfacing of a subsurface H atom initially placed directly under a surface methyl group or surface-bound H atoms did not, in 14 statistically independent trajectories, lead to associative desorption. Instead, the surface species either moves out of the way by hopping to other surface sites before the subsurface H atom hops out to the surface or the subsurface atom hops to adjacent subsurface sites before hopping out into a vacant surface site. The basic reason for this seems to be that the surface Ni atoms can only catalyze H–H and H–CH₃ bond formation/rupture on the exposed, undercoordinated side. There is, furthermore, a small but significant repulsive interaction between a subsurface H atom and a surface methyl group. Experimentally, enhanced reactivity in the presence of subsurface hydrogen has been observed,^{5,10} but these experiments were carried out with high coverage of both surface and subsurface species and the effect is likely due to the local energy release of surfacing H atoms resulting from the high-energy, nonequilibrium initial state. In our classical dynamics simulations the excess kinetic energy of a H atom after hopping out to a surface site dropped very quickly, on the time scale of 200 fs, and no associative process was observed in 14 trajectories. It is quite likely that a classical description of these processes is not adequate. It is, however, clear that under thermal conditions, the probability

of finding an energetic atom on the surface is not affected by the presence of H atoms in subsurface sites. The probability of finding an atom with energy E is only related to the Boltzmann factor $e^{-E/kT}$. The presence of an unstable state such as the subsurface hydrogen species does not increase the probability of finding a hot hydrogen atom on the surface under thermal conditions.

Our calculations also provide information about associative desorption of CH₄ and H₂ starting with surface species. In the saddle-point configuration for CH₄ desorption, the underlying Ni atom is lifted up from the surface plane by 0.25 Å. This reduces the energy of the saddle-point configuration in a way that is analogous to strain effects.²⁶ An analysis of classical trajectories for desorption showed that about 15% of the saddle-point energy goes into surface vibrational modes as the Ni atom relaxes back to its original position. The rest of the energy is taken up by the methane molecule and the majority, 60% of the total goes into translation, while vibration and rotation take up 20% and 5%, respectively. The symmetric and asymmetric stretches are found to be the most important vibrational modes. The principle of time reversal symmetry can be used to argue that these modes will also be most important for enhancing dissociative adsorption of methane on Ni(111), in agreement with recent experiments of Smith *et al.*³¹ and Juurlink *et al.*³²

ACKNOWLEDGMENTS

We would like to thank Fernando Vila for helping with the normal-mode analysis, as well as Bruce Kay and Art Voter for their helpful discussions. This work was funded by the U.S. Department of Energy, Division of Materials Research, by RANNIS, the Icelandic Center for Research, and the Robert A. Welch Foundation under Grant No. F-1601.

APPENDIX: CONVERGENCE

The sensitivity of the CH₄ dissociation barrier on Ni(111) to various computational parameters is given in Table III. For each parameter, the energy difference is with respect to our most accurate calculation described above. The most sensitive computational parameter in our calculation is k -point sampling. Given more computing power, this should be increased to verify convergence. For the smaller, four-atom-per-layer system, in which k -point sampling will

TABLE III. Sensitivity of the CH₄ dissociation energy barrier on Ni(111) with respect to computational parameters. Energy differences are with respect to a five-layer, nine nickel atoms per layer slab with the bottom two layers frozen, a plane-wave energy cutoff of 350 eV, a $2 \times 2 \times 1$ Monkhost-Pack k -point mesh, and spin-polarized calculation for which an activation energy barrier of 0.82 eV was calculated.

Energy (eV)	Computational parameter
0.30	k -point sampling (Γ to $2 \times 2 \times 1$)
0.25	Spin polarization
0.15	Surface relaxation (frozen to relaxed)
0.10	System size (four to nine atoms per layer)
0.05	Number of surface layers (four to five)
0.02	Plane-wave energy cutoff (240–350 eV)

be even more important, going from a $2 \times 2 \times 1$ Monkhost-Pack k -point mesh to a $4 \times 4 \times 1$ mesh did not change the binding energies by more than 0.1 eV. Spin polarization also plays a significant role, raising the barrier by 30%. Finally, surface relaxation and the number of layers in the Ni(111) slab are both needed to allow the large surface relaxation found at the transition state and to lower the barrier by 20%.

- ¹R. C. Egeberg, S. Ullmann, I. Alstrup, C. B. Mullins, and I. Chorkendorff, *Surf. Sci.* **497**, 183 (2001).
- ²J. T. P. Beebe, D. W. Goodman, B. D. Kay, and J. J. T. Yates, *J. Chem. Phys.* **87**, 2305 (1987).
- ³H. Yang and J. L. Whitten, *J. Chem. Phys.* **96**, 5529 (1992).
- ⁴H. S. Bengaard, J. K. Nørskov, J. Sehested, L. P. Nielsen, A. M. Molenbroek, and J. Rostrup-Nielsen, *J. Catal.* **209**, 365 (2002).
- ⁵A. D. Johnson, S. P. Daley, A. L. Utz, and S. T. Ceyer, *Science* **257**, 223 (1992).
- ⁶S. P. Daley, A. L. Utz, T. R. Trautman, and S. T. Ceyer, *J. Am. Chem. Soc.* **116**, 6001 (1994).
- ⁷V. Ledentu, W. Dong, and P. Sautet, *J. Am. Chem. Soc.* **122**, 1796 (2000).
- ⁸A. Michaelides, P. Hu, and A. Alavi, *J. Chem. Phys.* **111**, 1343 (1999).
- ⁹S. Wright, J. F. Skelly, and A. Hodgson, *Faraday Discuss.* **117**, 133 (2000).
- ¹⁰S. Wright, J. F. Skelly, and A. Hodgson, *Chem. Phys. Lett.* **364**, 522 (2002).
- ¹¹G. Mills, H. Jónsson, and G. K. Schenter, *Surf. Sci.* **324**, 305 (1995).
- ¹²G. Kresse and J. Hafner, *Phys. Rev. B* **49**, 14251 (1994).
- ¹³G. Kresse and J. Hafner, *Phys. Rev. B* **47**, R558 (1993).
- ¹⁴G. Kresse and J. Furthmüller, *Comput. Mater. Sci.* **6**, 15 (1996).
- ¹⁵J. P. Perdew, in *Electronic Structure of Solids*, edited by P. Ziesche and H. Eschrig (Akademie, Berlin, 1991).
- ¹⁶D. Vanderbilt, *Phys. Rev. B* **41**, 7892 (1990).
- ¹⁷H. Jónsson, G. Mills, and K. W. Jacobsen, in *Classical and Quantum Dynamics in Condensed Phase Simulations*, edited by B. J. Berne, G. Ciccotti, and D. F. Coker (World Scientific, Singapore, 1998), p. 385.
- ¹⁸G. Henkelman and H. Jónsson, *J. Chem. Phys.* **113**, 9978 (2000).
- ¹⁹G. Henkelman, B. P. Uberuaga, and H. Jónsson, *J. Chem. Phys.* **113**, 9901 (2000).
- ²⁰G. Henkelman and H. Jónsson, *J. Chem. Phys.* **111**, 7010 (1999).
- ²¹The conjugate-gradient method is an efficient algorithm for optimizing saddle-point structures in combination with the nudged elastic band and min-mode following methods (e.g., the dimer method). However, the force projections used in these methods can be problematic for a traditional implementation of the conjugate-gradient algorithm because there is no energy consistent with the projected forces. Instead, we use a modified conjugate-gradient method in which line minimizations are done using a single Newton's method iteration. The gradient of the force along the line is evaluated with a finite difference step, and the step size required to zero that force is estimated with a linear approximation. This force-only conjugate-gradient method is recommended for both saddle-point finding methods and standard geometry optimizations.
- ²²K. Christmann, *J. Chem. Phys.* **88**, 519 (1979).
- ²³J. Greeley and M. Mavrikakis, *Surf. Sci.* **540**, 215 (2003).
- ²⁴G. Kresse, *Phys. Rev. B* **62**, 8295 (2000).
- ²⁵G. Kresse and J. Hafner, *Surf. Sci.* **459**, 287 (2000).
- ²⁶M. Mavrikakis, B. Hammer, and J. K. Nørskov, *Phys. Rev. Lett.* **81**, 2819 (1998).
- ²⁷G. Henkelman and H. Jónsson, *Phys. Rev. Lett.* **86**, 664 (2001).
- ²⁸A. Eichler, repeated the methane dissociation on Ir(111) calculations reported in *Phys. Rev. Lett.* **84**, 664 (2001) and found that the system size effects are largely due to the limitation of the k -point sampling; The converged barrier is approximately 0.7 eV and not 0.3 eV as reported. (private communication).
- ²⁹J. C. Polanyi and W. H. Wong, *J. Chem. Phys.* **51**, 1439 (1969).
- ³⁰M. J. Frisch, G. W. Trucks, H. B. Schlegel *et al.*, *GAUSSIAN 98, Revision A.7*, Gaussian, Inc., Pittsburgh, PA, 1998.
- ³¹R. R. Smith, D. R. Killelea, D. F. DelSesto, and A. L. Utz, *Science* **304**, 992 (2004).
- ³²L. B. F. Juurlink, R. R. Smith, D. R. Killelea, and A. L. Utz, *Phys. Rev. Lett.* **94**, 208303 (2005).
- ³³T. Klamroth and P. Saalfrank, *J. Chem. Phys.* **112**, 10571 (2000).
- ³⁴J. Strömquist, L. Bengtsson, M. Persson, and B. Hammer, *Surf. Sci.* **397**, 382 (1998).
- ³⁵J. R. Trail, D. M. Bird, M. Persson, and S. Holloway, *J. Chem. Phys.* **119**, 4539 (2003).
- ³⁶C. L. A. Lamont, B. N. J. Persson, and G. P. Williams, *Chem. Phys. Lett.* **243**, 429 (1995).
- ³⁷A. Michaelides and P. Hu, *Surf. Sci.* **437**, 362 (1999).
- ³⁸C. Wert and C. Zener, *Phys. Rev.* **76**, 1169 (1949).
- ³⁹G. H. Vineyard, *J. Phys. Chem. Solids* **3**, 121 (1957).
- ⁴⁰E. Wigner, *Trans. Faraday Soc.* **34**, 29 (1938).
- ⁴¹E. Wigner, *Z. Phys. Chem. Abt. B* **19**, 203 (1932).
- ⁴²M. J. Gillan, *Phys. Rev. Lett.* **58**, 563 (1987).